Title Page

Shielding effectiveness of x-ray protective garment

H. Eder[a], H. Schlattl[b]

[a]Formerly Bavarian Environment Agency, priv. Am Stadtpark 43, D-81243 München,
T. 0152-01823802 eder-h@arcor.de (corresponding author)

[b]Helmholtz Zentrum München
Deutsches Forschungszentrum für Gesundheit und Umwelt (GmbH)
Ingolstädter Landstraße 1
D-85764 Neuherberg
Phone: +49 89 3187-0 helmut.schlattl@t-online.de

Shielding effectiveness of X-ray protective garment

Abstract

Purpose

Certification of the X-ray shielding garment is based on attenuation testing on flat material samples. We investigated the difference of shielding effectiveness compared to realistic use when the garment is worn on the body of a staff person.

Methods

Attenuation factors of X-ray protective aprons have been evaluated for several clinical scenarios with Monte Carlo (MC) calculations based on the ICRP female reference model and an experimental setup. The MC calculated attenuation factors refer to the effective dose *E*, whereas the measured attenuation factors refer to the personal dose equivalent *Hp(10)*. The calculated/measured factors were compared to the attenuation factors of the identical materials measured under the conditions of the standard IEC 61331-1 that is currently in use for the type testing of X-ray protective aprons.

Results

As a result, for example, at a common tube voltage of 80 kV, the real attenuation factors of a 0.35 mm Pb apron worn by a 3-dimensional body were 38% to 76% higher than when measured under IEC conditions on flat samples. The MC-calculated organ doses show the maximum contribution to *E* being within the operator´s abdomen/pelvis region.

Conclusions

With our findings, personal X-ray protective garments could be improved in effectiveness

Keywords: protective garment, attenuation factor, effective dose, organ doses

1. Introduction

The attenuation properties of X-ray protective aprons and other garments in practical use are rather complex. In the past, physical investigations have focused on their material properties, particularly lead-free and lead-composite protective clothing [1,2]. What remains to be investigated and put forth is a quantification of the actual attenuation of shielding materials in a realistic environment during clinical use. X-ray protective garments must be manufactured in accordance with the actual international standard IEC 61331-3:2014 [3] wherein the standard lead equivalence values (LEVs) of 0.25 mm Pb, 0.35 mm Pb and 0.50 mm Pb have been stated. Type testing of the shielding properties according to the European Personal Protective Equipment (PPE)-regulations [4] and other standards [5] is conducted under beam geometries defined in IEC 61331-1:2014 [6]. Generally, the test procedures demand a broad beam geometry with vertical incidence on a flat sample. In clinical practice, however, scatter radiation originating from the patient impinges on the body of a protected staff person at various angles, leading to longer path lengths for non-vertical incidence as illustrated in Fig. 1. Moreover, the bodies of the staff persons are more equal to cylindric or ellipsoidal surfaces than flat planes. Therefore, it can be assumed that a perpendicular incidence on the apron and the staff's body occurs only in very small regions of the body surface, thus potentially increasing the efficacy of the protective garment. A better understanding of the actual protection efficacy will allow the optimisation of the disposal of protective material around the body.

>> **Fig. 1**

Recent literature provides only a few references concerning the effective shielding properties of X-ray protective garment in clinical use. Hiroshige et al. [7] tested seven X-ray protective aprons specified as 0.25 mm, 0.35 mm and 0.50 mm LEVs in an experimental and practical field evaluation. Apart from the predictions based on physical transmission measurements, the personal dose equivalent measurements during the interventional procedures resulted in scanty shielding effects. Aprons specified as 0.25 mm Pb and 0.35 mm Pb showed small differences in the protection level. An explanation for this somewhat odd result has not been provided by the authors. Other publications report a reduced shielding efficacy due to material lesions and an inadequate body-fit of the protective aprons [8,9].

Saldarriaga Vargas et al. evaluated effective doses when wearing radioprotective garments [10]. Their findings are based on a whole-body exposure of the reference phantom defined in ICRP publication 110, [11]. The phantom was covered with a 0.5 mm Pb apron and exposed to a unidirectional X-ray field with discrete photon energies. Their results show the effect of inclined incidence on the effective dose but the potentially higher shielding effect is obviously covered there through the impact of unprotected parts of the body.

In the field of patient shielding during X-ray examinations, such as computed tomography (CT), new methods for shielding single radiosensitive body parts, such as the breast, against primary and scatter radiation were conducted [12].

Our current work focuses on the effect of realistic spatial incidence of X-ray scatter radiation on the protective clothing worn by the radiological staff persons, especially investigators and operators standing close to the patient. Attenuation factors and LEVs should be higher in practical use than those measured under the conditions of the IEC standard with a perpendicular incidence to the test material.

To provide numerical results for the protection efficiency, two approaches were followed:

First, the attenuation factors of aprons with LEV 0.25 mm / 0.35 mm / 0.50 mm worn by an Alderson Rando male phantom—representing the operator—were determined at tube voltages of 80 kV,100 kV and 120 kV, respectively. For this, *Hp(10)* dosimeters were arranged on the front of the phantom torso to provide mean personal dose equivalents under the scatter radiation from a water phantom, representing the patient. Measurements on the operator phantom were performed with various distances from the scatter volume under frontal as well as under a 30° rotated orientation.

Second, the effect of inclined incidence on the effective dose *E* was calculated for an ICRP female reference phantom utilising MC simulations for various additional conditions.

Finally, we asked for an optimised material disposition around the user's body for radiosensitive organs and tissues.

2. Materials and methods

<u>Nomenclature</u>

LEV lead equivalence value, expressed in mm Pb

E effective dose

Hp(10) personal dose equivalent

F_E attenuation factor of the shielding material based on *E*

$F_{Hp(10)}$ attenuation factor of the shielding material based on *Hp(10)*

F_{IEC} attenuation factor of the shielding material based on the IEC standard

CA_{hor} horizontal C-arm geometry: beam horizontal, patient standing

CA_{vert} vertical C-arm geometry: beam vertical, patient in a supine position on the table

DAP dose area product (Gy*cm²)

DR dosimeter reading

MC Monte Carlo calculation

patient phantom water phantom 25×25×15 cm³ (DIN 6815)

operator phantom Alderson Rando male phantom (measurements) and ICRP reference female phantom (MC simulation) with orientations:

frontal operator directly facing the patient

ROT30° operator turned by 30° around his/her vertical axis to the right

α azimuthal-angle coordinate of photon on the shielding cylinder

z height coordinate of photon on the shielding cylinder

φ azimuthal-angle direction of photon emerging from the shielding cylinder

ϑ polar-angle direction of photon emerging from the shielding cylinder

2.1 Laboratory measurements

2.1.1 Setup

Laboratory measurements were conducted on a stationary X-ray unit Titan E (GE), producing a horizontal cone beam with its central beam height fixed 120 cm above the floor (corresponding to CA_{hor}). To eliminate the adverse impact of leakage radiation from the tube housing, the X-ray containment was shielded additionally with an 8 mm lead. The beam quality was defined through tube voltage and an additional filtration of 2.5 mm Al. According to DIN 6815 [13], a water phantom with a length of 25 cm, width of 15 cm and height of 25 cm was located with the entrance plane being 100 cm from the focus and the centre being 120 cm above floor (Fig. 2), thus representing the exposure geometry during an X-ray examination of the trunk. The diameter of the circular field at the phantom entrance plane was 20 cm. An Alderson Rando male phantom, representing the operator, was positioned upright in a right angle to the centre beam facing the water phantom (phantom incidence direction frontal). The centre of the torso was positioned at the level of the centre beam. Distances between the water phantom and operator phantom were chosen as 30 cm and 60 cm, representing an operator standing near the patient and an assistance person, respectively. To investigate a position when the operator turns around his/her vertical axis, the operator phantom was additionally rotated by 30° (phantom incidence direction ROT30°) (Fig. 2). An overview of the investigated experimental scenarios is provided in Table 1.

>>**Fig 2**

2.1.2 Dosimeters

The operator phantom was equipped with four calibrated *Hp(10)* personal dosimeters EPD Truedose (Thermo Fisher Scientific™) positioned at the sternum (A), in front of both lungs (B, D) and at the centre of the abdomen (C) (Fig. 3). Each detector was orientated at its actual position tangentially to the phantom surface. The mean value of the four dosimeter readings should provide a mean personal dose equivalent *Hp(10)* as an average over the phantom torso and also an estimate of the effective dose [14]. During all test measurements, the dosimeters remained in their position on the skin surface in order to also detect the backscatter of the body. This is an important criterion to measure the relevant *Hp(10)* doses [15].

>>**Fig.3**

2.1.3 Attenuation measurements

X-ray protective sheets of pure lead polymer material were taken from commercially available aprons with nominal LEVs of 0.25 mm, 0.35 mm and 0.50 mm LEV and prepared to cover the phantom body. Before each measurement, it was ensured that the shielding material was positioned flat on each of the detectors.

First, attenuation ratios, LEVs and attenuation factors F_{IEC} of the shielding materials were evaluated for flat samples according to the IEC standard at 80 kV /100 kV /120 kV tube voltage. Identical tube voltages were applied for the measurements of the *Hp(10)* doses at the operator phantom surface with and without the shielding sheets. From this, the mean attenuation factors were calculated.

2.2 Monte Carlo Simulations

The particle transport in the water phantom (patient) and the ICRP reference female model (operator) (ref. [11]) were simulated with a user code to the Monte Carlo transport code EGSnrc in version V4-2-3-0 [16]. The technical simulation parameters of the code and the physics used agree with those of [17]. For instance, photons (electrons) are followed until their energy drops below 2 keV (20 keV), where the remaining kinetic energy is then deposited locally. For active bone marrow and endosteum, dose coefficients are deduced by applying the so-called 3-factor formalism [18], where the dose enhancement factors are taken from ICRP Publication 116 [19]. The soundness of the Monte Carlo code in providing accurate dose values has been verified [20]. The X-ray spectra have been obtained using SpekCalc [21] for all the cases of Table 1.

The simulation of the exposure scenario has been divided into three steps and is sketched in Fig. 4:

I. Irradiation of the patient and recording of all the emitted photons traversing the virtual plane in a 20 cm distance.
II. Projecting the trajectories of the recorded photons on a cylindrical apron and reducing the statistical particle weight proportional to the attenuation caused by the particle track length through the apron.
III. Exposing the operator with the resulting field of attenuated scatter photons and computing organ and effective doses [22].

In step I, the symmetry of the emitted scatter field is exploited by mapping photons emitted from the left and bottom border of the water phantom to the right and top border, respectively. Since the virtual scoring plane can be rotated, only one simulation is necessary to obtain both the CA_{hor} as well as the CA_{vert} case. In step II, no Monte Carlo simulation is performed, i.e., scattering in the air and apron are ignored. For patient-operator distances of 30 cm and 60 cm, the results of step II are the distribution functions $\Phi(\alpha, z, \varphi, \vartheta, E)$ of photons emitted by the cylindrical apron, where α (azimuthal angle of the shielding cylinder) and z (height coordinate of the shielding cylinder) define the position of the photon in the cylinder coordinates, φ and ϑ are the azimuthal and the polar angles, respectively, of the particle direction in the spherical reference system and E is the particle energy. The distribution functions Φ are then used to sample the distribution of the photons impinging on the operator being oriented either frontal or ROT30°. The effective dose is computed from the organ doses using the weighting factors of ICRP Publication 103 [22].

The diameter and position of the cylindrical apron have been fitted to the model such that it closely encircles the waist of the model. The apron extends from the bottom to the top of the model. Since the arms are not inside the apron, they have been removed from the model. The setup for CA_{vert}, operator irradiated frontal at a distance of 30 cm is depicted in Fig. 4. An overview of the MC-investigated scenarios is shown in Table 1 and Fig. 5. Table 1 also contains the beam conditions of computed tomography (CT). For the beam directions CA_{vert} and CA_{hor}, the centre of the phantom was positioned at a height of 87.5 cm above the floor. Effective doses and attenuation factors were calculated without and with in situ shieldings of 0.25 mm Pb / 0.35 mm Pb / 0.50 mm Pb. Further, the organ doses and their contribution to the effective dose E were calculated for the tube voltage of 100 kV both with and without 0.25 mm Pb shielding. As a special scenario, an additional shielding of the lower body was investigated.

>> **Fig.4**

>> **Table 1**

>> **Fig 5**

3. Results

3.1 IEC attenuation factors

The measured attenuation factors F_{IEC}, based on the IEC standard, of the shieldings applied to the operator phantom are shown in Table 2. It has been proved that the factors comply with the nominal LEVs.

3.2 Phantom measurements

Depending on the orientation of the operator phantom, the four dosimeters A–D showed different readings. Especially in case of the ROT30° incidence—because of the different inclination of the photon paths to the protective material and anisotropy of the *Hp(10)* detectors—the readings differ (Fig. 6). Hence, for calculating the attenuation factors, the mean value of the four readings with and without shielding was considered.

>>**Fig.6**

Table 2 presents the attenuation factors $F_{Hp(10)}$ calculated as mean value from the four dosimeter readings with and without shielding material for the different scenarios described in Table 1. The *Hp(10)* based attenuation factors are significantly greater than the corresponding IEC factors presented in the same table. Hence the IEC rating underestimates the real attenuation in practical use.

3.3 Uncertainties of measurements

Uncertainties of the dose measurements were due to the dose reproducibility of the X-ray unit (exposition uncertainty) and the reproducibility of the dosimeter readings (response uncertainty). The standard deviation (SD) of the personal dosimeters readings was tested using repeated Cs137-Isotope expositions and resulted in a value of 0.9% (note: the EPD Truedose dosimeter is specified for the Gamma energy of 662 keV). For low doses in the range of 5 – 10 µSv, the dosimeter resolution of 0.1 µSv has also been considered (<2% resolution error). The SD of the X-ray expositions was 0.6% (tested by repeated measurements using a precision dosimeter). The total SD of the attenuation factors $F_{Hp(10)}$ was calculated by the error propagation law (2x exposition, 2x dosimeter response, 1x resolution for signal <10µSv), resulting in a value of 2.51%. The standard deviation of the IEC attenuation factors F_{IEC} was determined with reference lead foils (99.9% purity) and accounts to 2.5%. Hence, the SD of the ratio $F_{Hp(10)}/F_{IEC}$ results in 3.54 %. The determined SDs were not extra reported or depicted with the presentation of the measured data.

>>**Table 2**

3.4 Monte Carlo simulations

The attenuation factors F_E for horizontal (CA_{hor}) and vertical (CA_{vert}) beam geometry were calculated for different orientations of the operator reference phantom (frontal / ROT30°) and three tube voltages 80 kV / 100 kV / 120 kV. The results are reported in Table 2 together with the measured attenuation factors $F_{Hp(10)}$ and the IEC-factors.

Attenuation factors F_E were also evaluated for beam conditions used in the CT applications featuring higher filtrations, Table 2. It was found that the factors for a 60 cm distance between operator phantom and water phantom, are generally 5% – 10% lower than those for 30 cm.

The attenuation factors $F_{Hp(10)}$ and F_E were set in relation to the attenuation factors F_{IEC}, Table 3. The results disclose that the ratios F_E/F_{IEC} and $F_{Hp(10)}/F_{IEC}$, respectively, grow with an increasing LEV.

>>Table 3

Exemplified Fig. 7 shows the results for a 0.35 mm Pb apron and the common ROT30° modality depicted as a graph. The curves feature attenuation factors based on *Hp(10)* and *E*, compared to the IEC attenuation factors F_{IEC} measured on flat samples.

>>Fig. 7

3.5 Calculation of organ doses

As can be seen in the visualisation of the skin doses behind 0.25 mm Pb of the mathematical reference phantom (Fig. 8), mainly the organs in the region pelvis/abdomen are affected from the scatter radiation originating from the patient. The dose maximum for all the investigated scenarios occurs in the region at the tabletop level. At this body region, most of the radiosensitive tissues (colon, stomach, urinary bladder, red bone marrow) are situated. Table 4 presents the contributions of the individual organ doses to the effective dose for an operator standing near the patient in the case of a 100 kV tube voltage, ROT30° incidence, being unprotected and protected with 0.25 mm lead protection.

>>Fig 8

>>Table 4

3.6 Additional shielding of the lower body

From Table 4 it can be seen that the major part of *E* originates from the lower body. If the operator wears a 0.25 mm Pb all-over apron and the lower body is shielded additionally with a 0.25 mm Pb from the pubis to the sternum, attenuation factors F_E rise by 32% to 50 % compared to the attenuation factors of an all-over apron of 0.35 mm Pb featuring an approximately identical weight (Table 5 and Fig. 9). Additionally, if the breast is shielded, from Table 4 it can be seen that around 80% of the effective dose arises within this body region.

>>Table 5

>>Fig. 9

4. Discussion

As a result of the phantom measurements and MC-simulations, it can be stated that the attenuation factors of lead aprons based on the effective dose *E* and the personal dose equivalent *Hp(10)* are significantly higher than that measured according to the IEC standard. For a typical scenario during interventions (80 kV/ ROT30°/0.35 mm Pb), the attenuation factors are 38% / 76% (CA_{vert}/CA_{hor}) higher compared to the attenuation factors resulting from the IEC testing of flat samples. The enhancement is mainly due to the three-dimensional surface of the in-situ shielding causing longer transmission paths through the shielding material. Hence, attenuation factors and LEVs become effectively higher than that of the flat samples and a vertical incidence.

It can be stated that the attenuation factors resulting from the scenario ROT30° based on *Hp(10)* and the corresponding MC-calculated factors based on *E* (Fig. 7) are in good accordance. However, for the frontal scenario, the MC-evaluated attenuation factors range between the IEC and the *Hp(10)* based factors. The differences to the ROT30° scenario might be explained through the anatomic formed protective apron in the case of the Alderson phantom versus the cylindric shielding assumed for the MC-calculations. The individual location of the organs relative to the incident field and their different weighing factors may also explain the differences between F_E and $F_{Hp(10)}$

A real advantage of the shielding efficacy arises in the optimisation of material disposition with respect to organs with high w_T-factors as bladder, stomach, colon, gonads. Patients are mostly found in the supine position on the examination table, and thus, the source of scatter radiation is located directly vis-à-vis of the critical organs of the examiner/operator. It seems self-evident to concentrate the shielding material within this body region.
Following this approach, in the future, optimised shielding aprons providing equal protection with respect to *E* could be lighter than aprons with uniformly disposed shielding material.

5. Conclusions

Our results underpin the thesis that the attenuation of protective garment worn on the body is higher than that gained from the IEC compliant measurements on flat samples. Considering this factor, X-ray protective aprons, especially if they are optimised with respect to radiosensitive organs and the modalities of medical procedures, could be lighter than they are currently. In detail, a concentration of material covering the lower part of the body from the gonads to the breast, connected with a reduction of material on the remainder of the body could improve the protective efficacy and/or lower the weight.

Acknowledgements

We are grateful to the Bavarian State Office of Weights and Measures for supporting the measurements and granting the use of the radiation laboratory.

References

[1] Bartal G, Sailer AM, Vano E. Should we keep the lead in the aprons? Techniques in Vascular and Interventional Radiology 2018;21(1): 2-6 https://DOI.org/10.1053/j.tvir.2017.12.002.

[2] McCaffrey JP, Tessier F, Shen H. Radiation shielding materials and radiation scatter effects for interventional radiology (IR) physicians. Med. Phys. 2012;39(7):4537-46.

[3] International Electrotechnical Commission. Protective devices against diagnostic medical X-radiation, IEC 61331 Part 3: Protective clothing, eyewear and protective patient shields; 2014.

[4] Regulation (EU) 2016/425 on personal protective equipment. Latest update: 08/10/2020.

[5] ASTM F3094-14 Standard Test Method for Determining Protection Provided by X-ray Shielding Garments Used in X-ray Fluoroscopy from Sources of Scattered X-Rays. ASTM International; 2014.

[6] International Electrotechnical Commission IEC. Protective devices against diagnostic medical X-radiation. IEC 61331 Part 1: Determination of attenuation properties of materials; 2014.

[7] Hiroshige M, Koshida K, Ishigamori O et al. Evaluation of the effectiveness of x-ray protective aprons in experimental and practical fields. Radiol. Phys. Technol. 2014;7(1):158-66.

[8] Franken Y, Huyskens C J. Guidance on the use of protective lead aprons in medical radiology. protection efficiency and correction factors for personal dosimetry. Conference 6th Workshop on Occupational Exposure Optimisation in the Medical and Radiopharmaceutical Sectors. Madrid; 2002.

[9] Sousha H A, Rabie N, Hassan G M. Experimental investigation of commercially available lead composite aprons used for diagnostic X-rays. Radiation Effects & Defects in Solids 2011;166(12):935-41. https://doi.org/10.1080/10420150.2011.559237

[10] Saldarriaga Vargas C, Struelens L, Vanhavere F. The challenges in the estimation of the effective dose when wearing radioprotective garments. Radiat. Prot. Dosim. 2018;178(1):101-11.

[11] ICRP, Adult Reference Computational Phantoms, ICRP Publication 110; 2009.

[12]Saba V, Keshtkar M. Targeted radiation energy modulation using Saba shielding reduces breast dose without degrading image quality during thoracic CT examinations. Physica Medica 2019;(65):238-46 https://doi.org/10.1016/j.ejmp.2019.05.013

[13] DIN 6815:2013 Medizinische Röntgenanlagen bis 300 kV – Regeln für die Prüfung des Strahlenschutzes nach Errichtung, Instandsetzung und wesentlicher Änderung. Berlin: Beuth; 2013.

[14] Berechnungsgrundlage für die Ermittlung von Körperdosen bei äußerer Strahlenexposition. Veröffentlichungen der Strahlenschutzkommission Band 43. Urban und Fischer; 3rd.edition 2017.

[15] Ginjaume M, Eleftheria C, Brodecki M et al. Effect of the radiation protective apron on the response of active and passive personal dosemeters used in interventional radiology and cardiology. Radiat. Prot. Dosim. 2019;178(1):101-11.

[16] I. Kawrakow E, Mainegra-Hing D, Rogers F. Tessier and B. Walters, The EGSnrc code system: Monte Carlo simulation of electron and photon transport. National Research Council of Canada. Ottawa; 2010.

[17] Schlattl H, Zankl M, Becker J, Hoeschen C. Dose Conversion Coefficient for Paediatric CT Examinations with Automatic Tube Current Modulation. Phys. Med. Biol. 2012;57:6309-26.

[18] Kramer R, Ermittlung von Konversionsfaktoren zwischen Körperdosen und relevanten Strahlungskenngrößen bei externer Röntgen- und Gamma-Bestrahlung. GSF–National Research Center for Environment and Health. Neuherberg; 1982.

[19] ICRP, Conversion Coefficients for Radiological Protection Quantities for External Radiation Exposures, ICRP Publication 116; 2010.

[20] Fehrmann M, Schlattl H, Schegerer A, Werncke T. Comparison of experimental and numerical methods of patient dose estimations in CT using anthropomorphic models. Rad. Prot. Dosim. 2020; 190(1):71-83.

[21] Poludniowski G, Landry G, DeBlois F, Evans P, Verhaegen F. SpekCalc: a program to calculate photon spectra from tungsten anode x-ray tubes. Phys. Med. Biol. 2009;54:N433-38.

[22] ICRP, The 2007 Recommendations of the International Commission on Radiological Protection, ICRP Publication 103; 2007.

Tables

Table 1 Overview on the different scenarios investigated with electronic dosimeter readings (DR) and Monte Carlo calculations (MC) employing an Alderson phantom and an ICRP female reference phantom, respectively, as operator phantom and a water phantom as patient phantom. Centre beam level was 87.5 cm for MC and 120 cm for DR.

Beam quality / mean energy	LEV of the applied shieldings (mm Pb)	Distance water phantom to operator phantom	Incidence rel. to the operator phantom	Beam direction (DR)	Dosi-metry DR	Beam direction (MC)	Dosi-metry MC
80 kV + 2.5 Al = 42.9 keV	0 0.25 0.35 0.50	30 cm	frontal	CA_{hor}	+	CA_{hor}/CA_{vert}	+
			ROT30°	CA_{hor}	+	CA_{hor}/CA_{vert}	+
		60 cm	frontal	CA_{hor}	+		o
			ROT30°		o		o
100 kV + 2.5 mm Al = 49.2 keV	0 0.25 0.35 0.50	30 cm	frontal	CA_{hor}	+	CA_{hor}/CA_{vert}	+
			ROT30°	CA_{hor}	+	CA_{hor}/CA_{vert}	+
		60 cm	frontal	CA_{hor}	+		o
			ROT30°		o		o
120 kV + 2.5 Al = 54.5 keV	0 0.25 0.35 0.50	30 cm	frontal	CA_{hor}	+	CA_{hor}/CA_{vert}	+
			ROT30°	CA_{hor}	+	CA_{hor}/CA_{vert}	+
		60 cm	frontal	CA_{hor}	+		o
			ROT30°		o		o
120 kV + 2.5 Al + 0.2 Cu = 63.5 keV	0 0.25 0.35 0.50	30 cm	frontal	Computed Tomography			+
			ROT30°				+
		60 cm	frontal				+
			ROT30°				+

Legend:
DR = Values from dosimeter reading
MC = Values from Monte Carlo simulations
o = Measurement/calculation not performed
+ = Measurement/calculation performed

Table 2 Attenuation factors $F_{Hp(10)}$ calculated from means of 4 *Hp(10)* dosimeter readings (DR) and attenuation factors F_E from MC-calculations (MC) under various scenarios (kV, distance water phantom – Alderson phantom (DR) or ICRP reference phantom (MC), beam incidence direction to the Alderson phantom (DR) or ICRP reference phantom (MC)) for 0.25/0.35/0.50 mm Pb shieldings. Outmost right column: Measured attenuation factors F_{IEC} on flat samples acc. to IEC 61331-1:2014

Beam quality / mean energy	LEV mm Pb	Method (see legend)	30 cm frontal	30 cm ROT30°	60 cm frontal	60 cm ROT30°	F_{IEC}
			- Attenuation factors -				
80 kV + 2.5 Al = 42.9 keV	0.25	DR	26.1	24.3	21.3	-	14.9
		MC	16.8 / 18.9	17.0 / 20.8	-	-	-
	0.35	DR	59.6	47.4	47.7	-	26.3
		MC	36.6 / 42.5	37.2 / 47.5	-	-	-
	0.50	DR	157.7	127.6	133.7	-	55
		MC	104.2 /125.2	105.9 / 143.3	-	-	-
100 kV + 2.5 mm Al = 49.2 keV	0.25	DR	13.7	13.2	12.7	-	8.85
		MC	9.6 / 10.6	9.7 / 11.3	-	-	-
	0.35	DR	26.7	24.4	24	-	14.2
		MC	17.5 / 19.8	17.7 / 21.4	-	-	-
	0.50	DR	56.5	49.8	47.6	-	26.0
		MC	38.5 / 44.8	39.1 / 49.5	-	-	-
120 kV + 2.5 mm Al = 54.5 keV	0.25	DR	10.2	10.3	8.8	-	6.7
		MC	8.0 / 8.2	8.0 / 8.6	-	-	-
	0.35	DR	17.9	16.1	15.0	-	10.4
		MC	14.1 / 14.5	14.2 / 15.4	-	-	-
	0.50	DR	36.8	33.1	30.0	-	18.9
		MC	29.3 / 30.0	29.5 / 32.1	-	-	-
120 kV + 2.5Al +0.2Cu = 63.5 keV	0.25	MC	7.1 / 7.2	7.1 / 7.5	6.4 / 6.7	6.5 / 6.9	-
	0.35		12.2 / 12.5	12.5 / 13.1	10.9 / 11.4	11.1 / 11.9	-
	0.50		25.2 / 25.6	25.7 / 26.9	22.0 / 23.0	22.4 / 24.1	-

Legend:
DR = Values from dosimeter readings (CA_{hor})
MC = Values from Monte Carlo simulations (CA_{vert} / $CA_{hor.}$)

Table 3 Ratios of attenuation factors F_E/F_{IEC}, and $F_{Hp(10)})/F_{IE}$. Denotation: CA_{vert} /CA_{hor}, single values: CA_{hor}

		0.25 mm Pb			0.35 mm Pb			0.50 mm Pb		
kV		frontal, 30 cm	frontal 60 cm	ROT30°, 30 cm	frontal, 30 cm	Frontal 60 cm	ROT30°, 30 cm	frontal, 30 cm	frontal 60 cm	ROT30°, 30 cm
80	DR	1.75	1.42	1.63	2.26	1.81	1.80	2.86	2.43	2.32
	MC	1.12/1,26		1.14/1.39	1.36/1.57		1.38/1.76	1.89/2.27		1.92/2.60
100	DR	1.54	1.43	1.49	1.88	1.69	1.71	2.17	1.83	1.91
	MC	1.08/1.20		1.10/1.27	1.23/1.39		1.25/1.51	1.48/1.72		1.50/1.90
120	DR	1.52	1.31	1.52	1.72	1.44	1.54	1.94	1.58	1.75
	MC	1.19/1.22		1.19/1.28	1.35/1.39		1.36 /1.47	1.55/1.59		1.56/1.70

Table 4 Contribution of organ doses (%) to *E* referring to the modalities of Fig. 5 (operator ROT30°) with no protection and with 0,25 mm Pb shielding, respectively. The bold figures show the contributions of organs/tissues from the lower part of the body. (*) only parts of the organs/tissues are situated in the lower body. w_T organ weighting factors acc. to ICRP 103 [22]

Operator ROT30°/100 kV		Contribution to effective dose *E*			
		no apron		0,25mm Pb	
	w_T	CA_{hor}	CA_{vert}	CA_{hor}	CA_{vert}
active bone marrow	0,12	**6,0%***	**5,9%***	**7,7%***	**7,2%***
colon wall	0,12	**22,6%**	**19,7%**	**24,8%**	**21,4%**
lungs	0,12	5,3%	6,0%	4,4%	5,7%
stomach wall	0,12	**17,0%**	**19,0%**	**17,1%**	**19,8%**
breast, total	0,12	13,6%	14,5%	7.4%	10,1%
remainder	0,12	**9,1%***	**9,9%***	**9,8%***	**10,2%***
gonads	0,08	**6,8%**	**5,7%**	**10,5%**	**8,3%**
urinary bladder wall	0,04	**10,8%**	**9,0%**	**11,5%**	**8,8%**
oesophagus	0,04	1,2%	1,4%	1,1%	1,5%
liver	0,04	**2,6%**	**2,6%**	**2,3%**	**2,6%**
thyroid	0,04	2,5%	2,7%	1,6%	2,1%
endosteum	0,01	0,6%	0,9%	0,8%	0,8%
brain	0,01	0,2%	0,2%	0,1%	0,2%
salivary glands	0,01	0,6%	0,8%	0,3%	0,5%
skin, total	0,01	1,2%	1,6%	0,8%	0,8%

Table 5 Attenuation factor F_E a) for a 0,35 mm Pb overall apron and b) a 0,25 mm Pb overall apron plus 0,25 mm additional shield of the lower body (Fig 9). Orientation and distance of the operator phantom is indicated. Denotation beam direction: CA_{vert} / CA_{hor}.

Tube voltage 100 kV	a) 0.35 mm Pb		b) 0,25 + 0,25 mm Pb	
	frontal 30 cm	ROT30°, 30 cm	frontal 30 cm	ROT30°, 30 cm
F_E	17,5/19,8	17,7/21,4	23,2/29,4	23,9/32,2

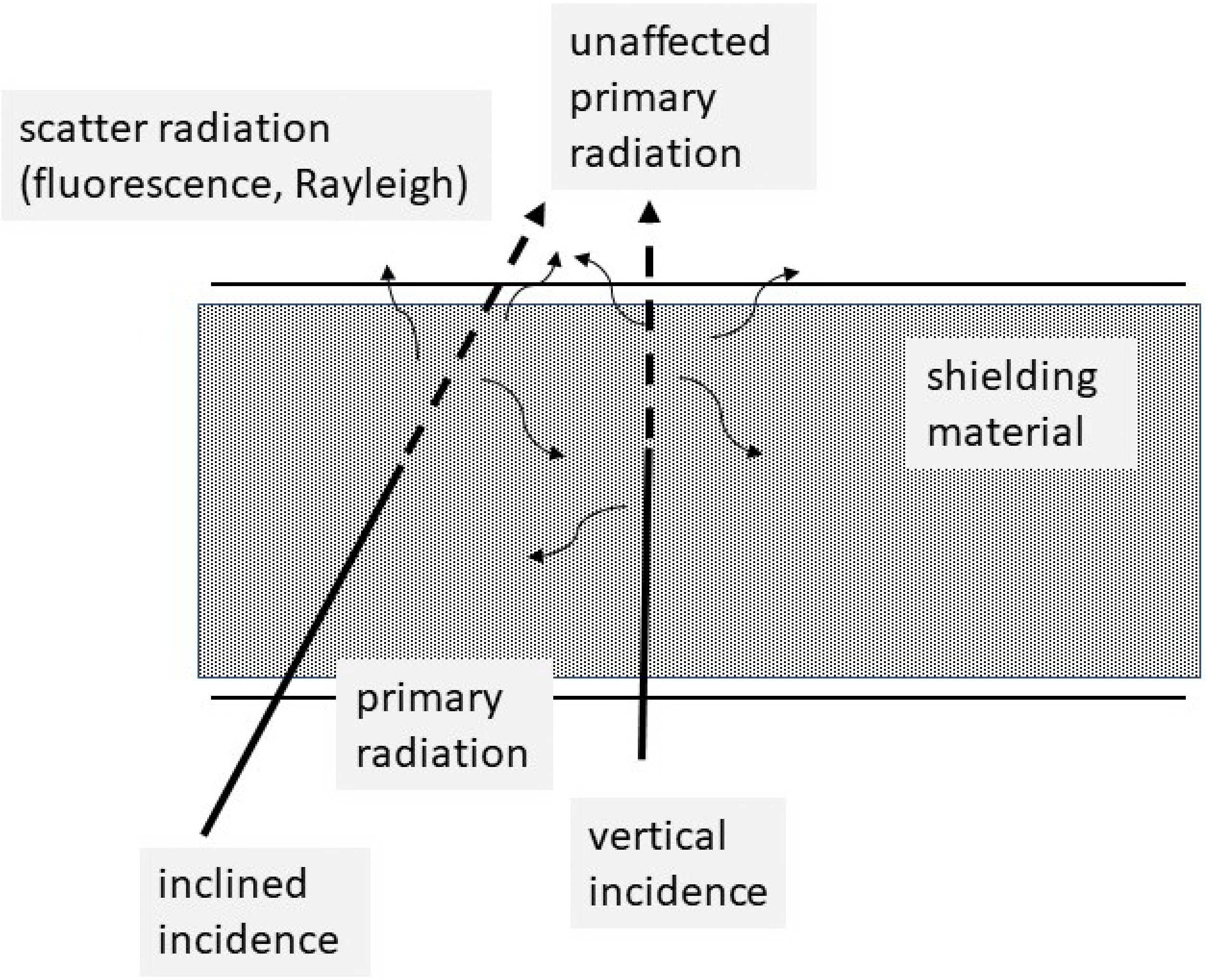
unaffected primary radiation
scatter radiation (fluorescence, Rayleigh)
shielding material
primary radiation
inclined incidence
vertical incidence

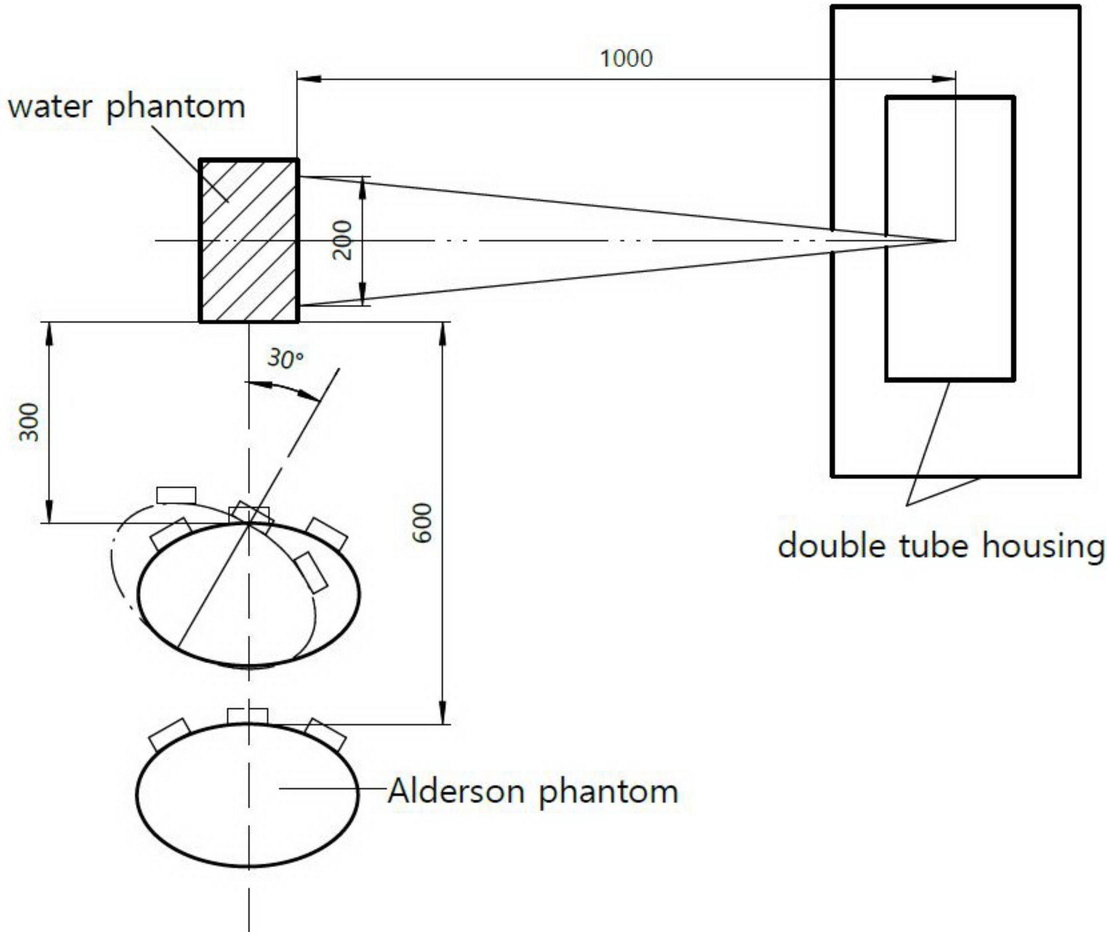

1000
water phantom
200
300
30°
600
double tube housing
Alderson phantom

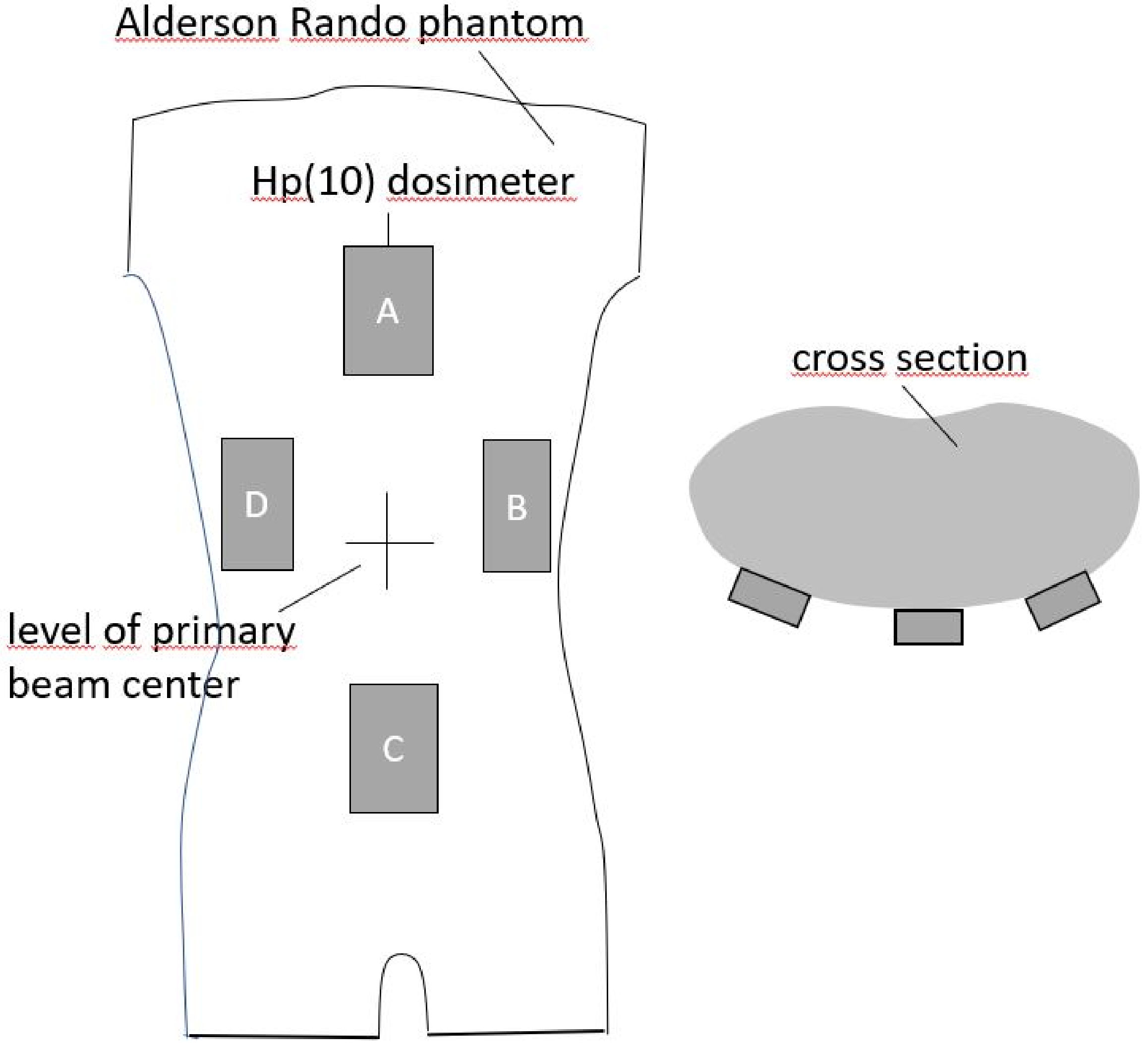
Alderson Rando phantom
Hp(10) dosimeter
A
D
B
C
level of primary beam center
cross section

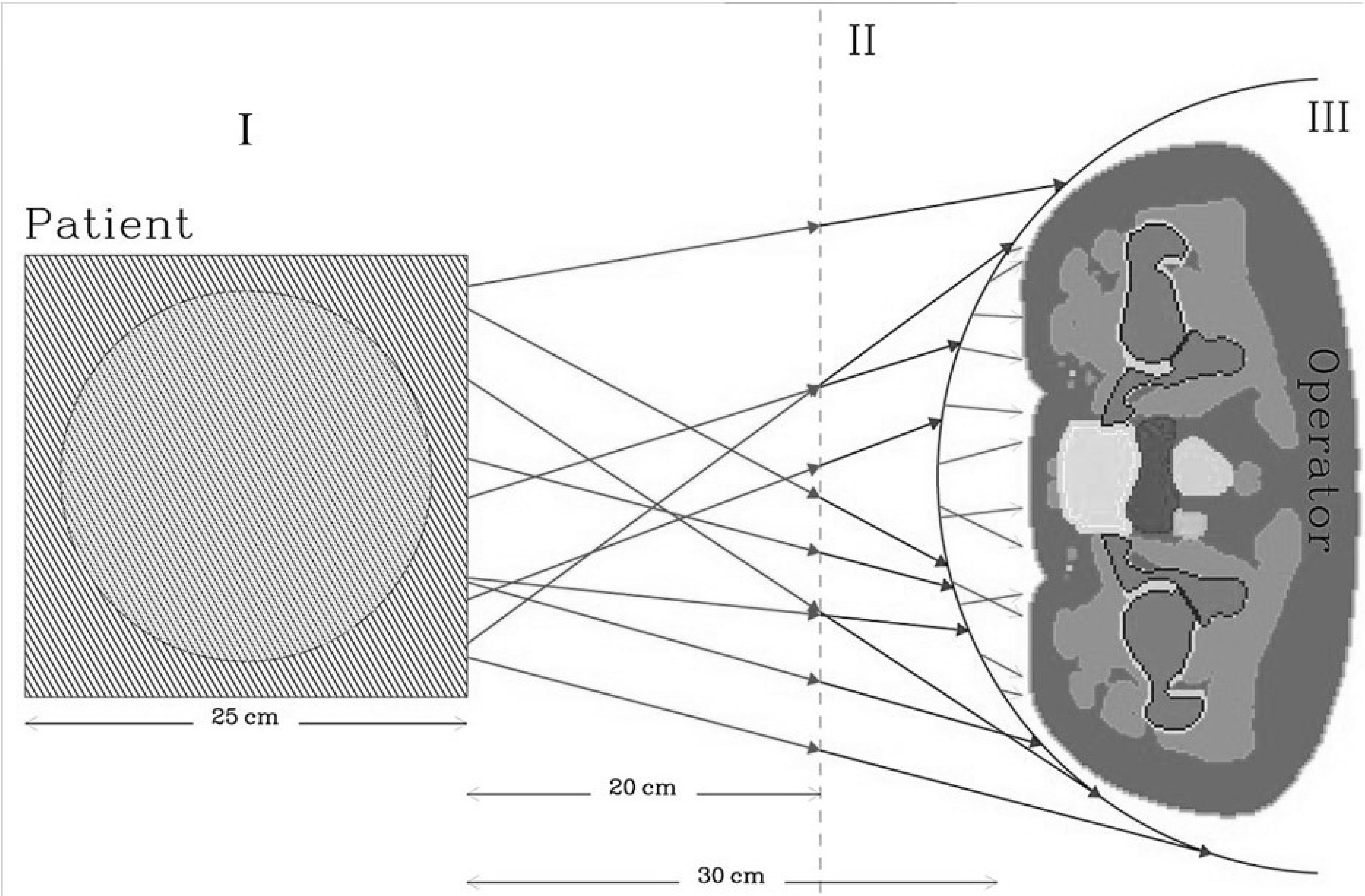

I
II
III
Patient
Operator
25 cm
20 cm
30 cm

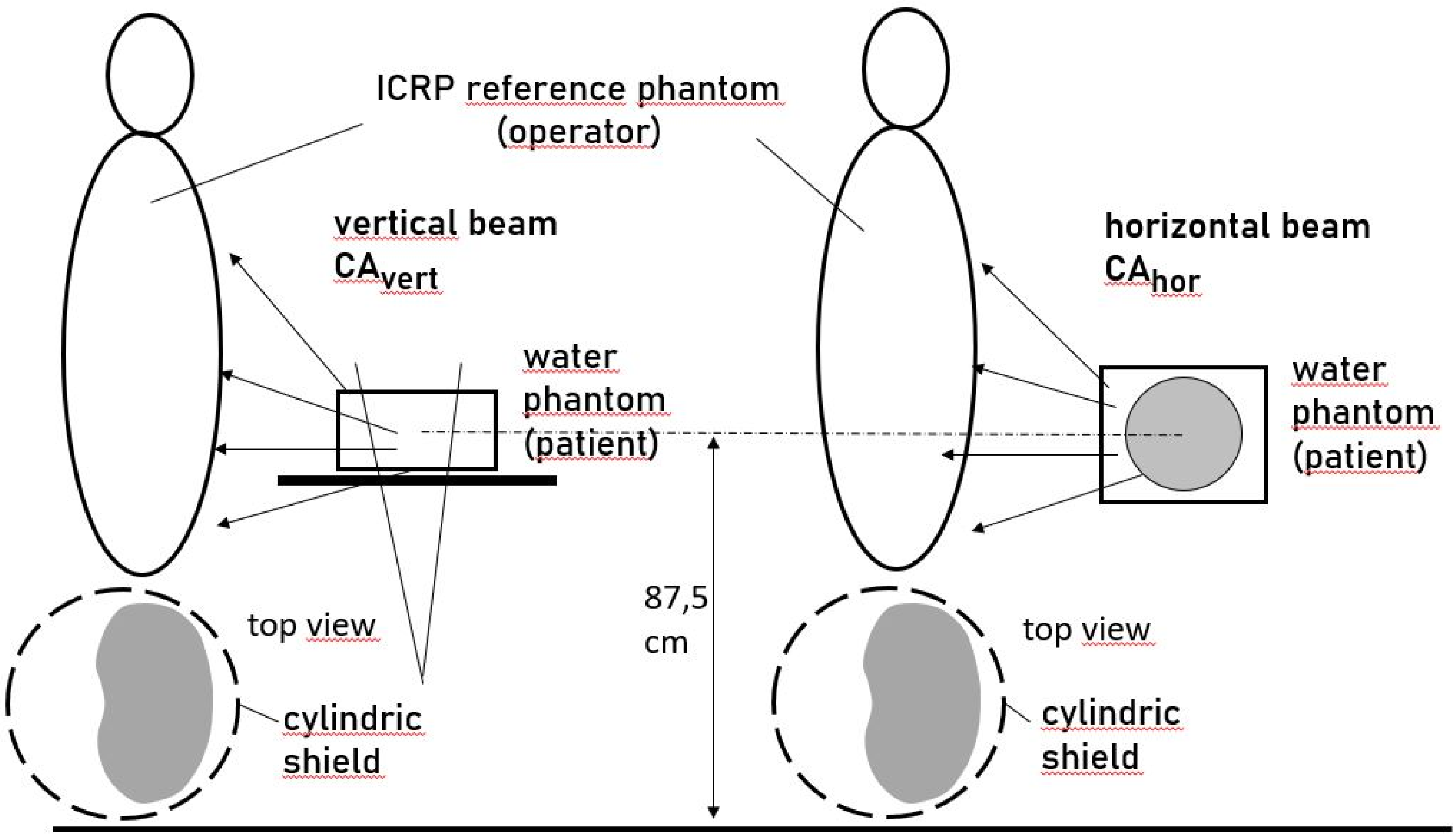
ICRP reference phantom
(operator)
vertical beam
CA$_{vert}$
water
phantom
(patient)
horizontal beam
CA$_{hor}$
water
phantom
(patient)
87,5
cm
top view
cylindric
shield
top view
cylindric
shield

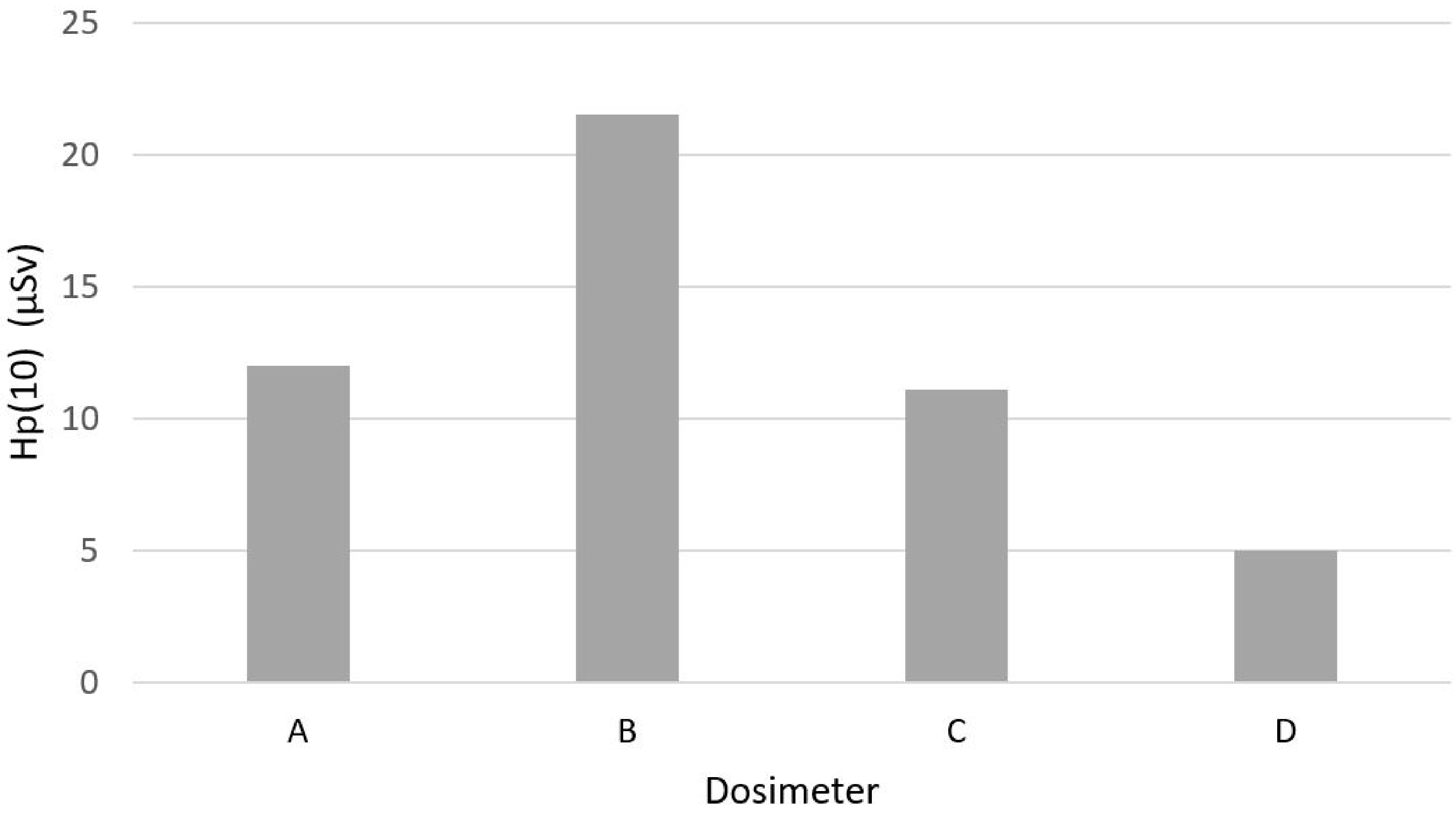
25
20
15
10
5
0
Hp(10) (μSv)
A
B
C
D
Dosimeter

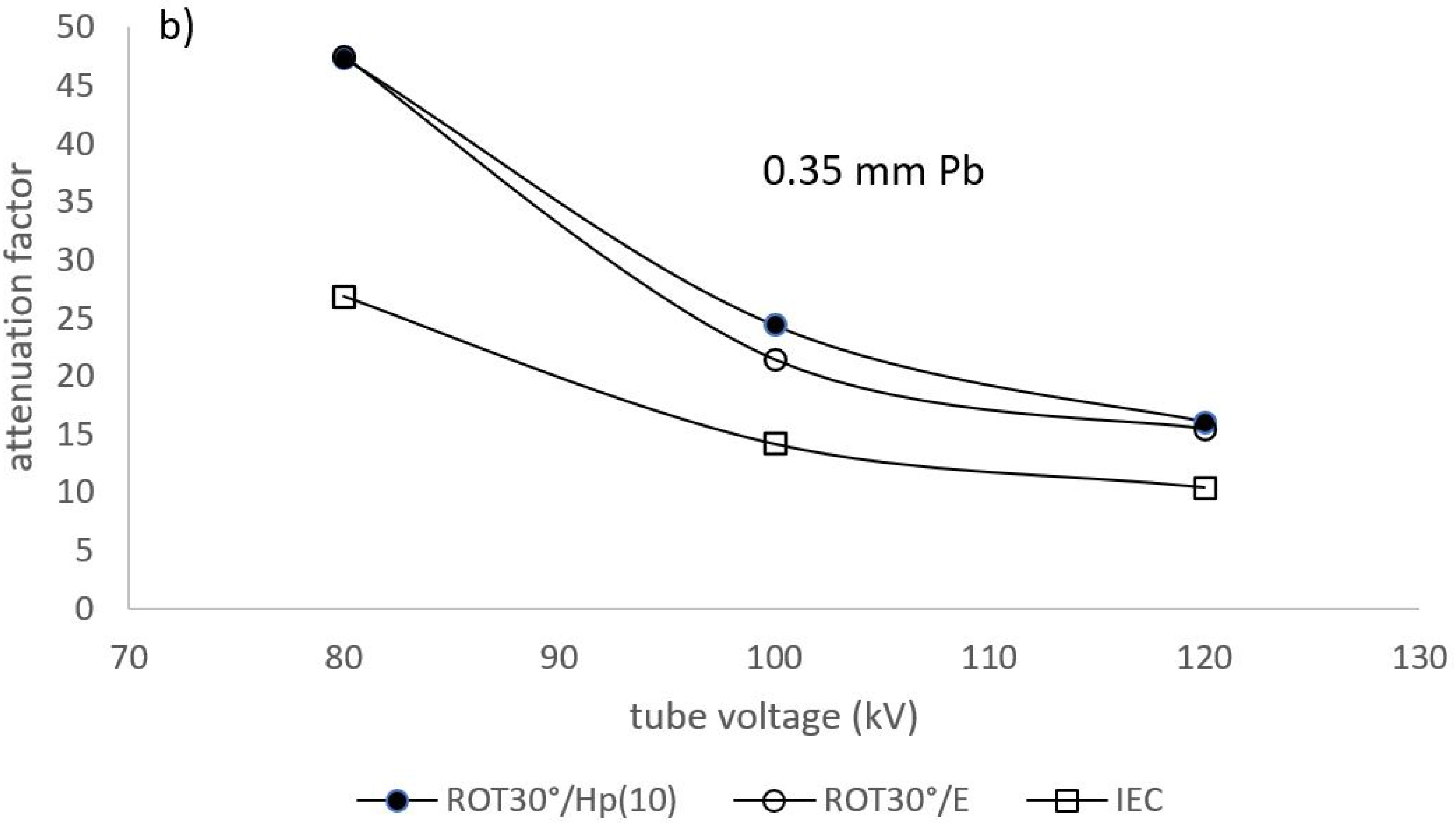
b)
0.35 mm Pb
attenuation factor
50
45
40
35
30
25
20
15
10
5
0
70
80
90
100
110
120
130
tube voltage (kV)
ROT30°/Hp(10)
ROT30°/E
IEC

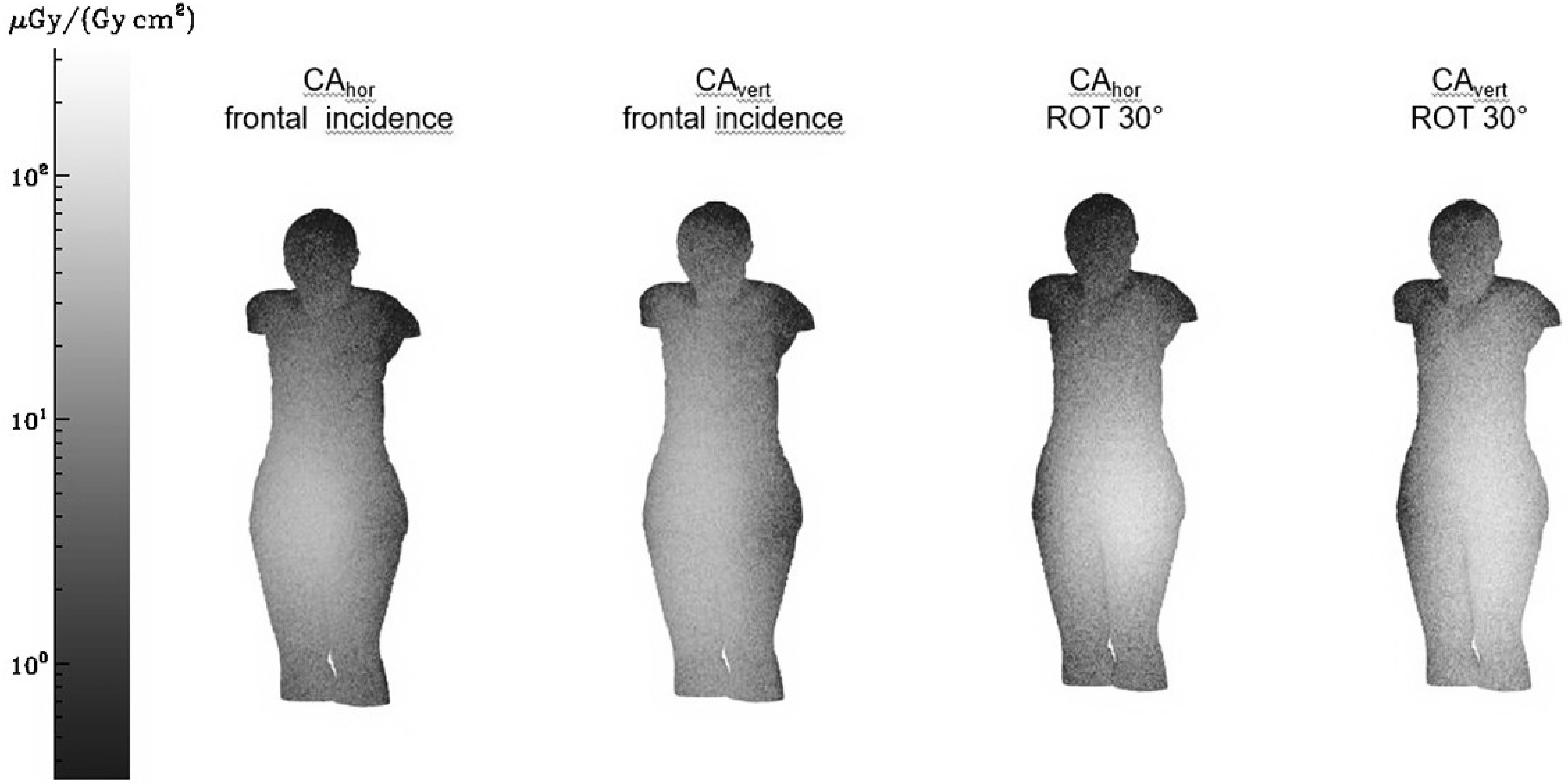

μGy/(Gy cm²)
10²
10¹
10⁰
CAhor
frontal incidence
CAvert
frontal incidence
CAhor
ROT 30°
CAvert
ROT 30°

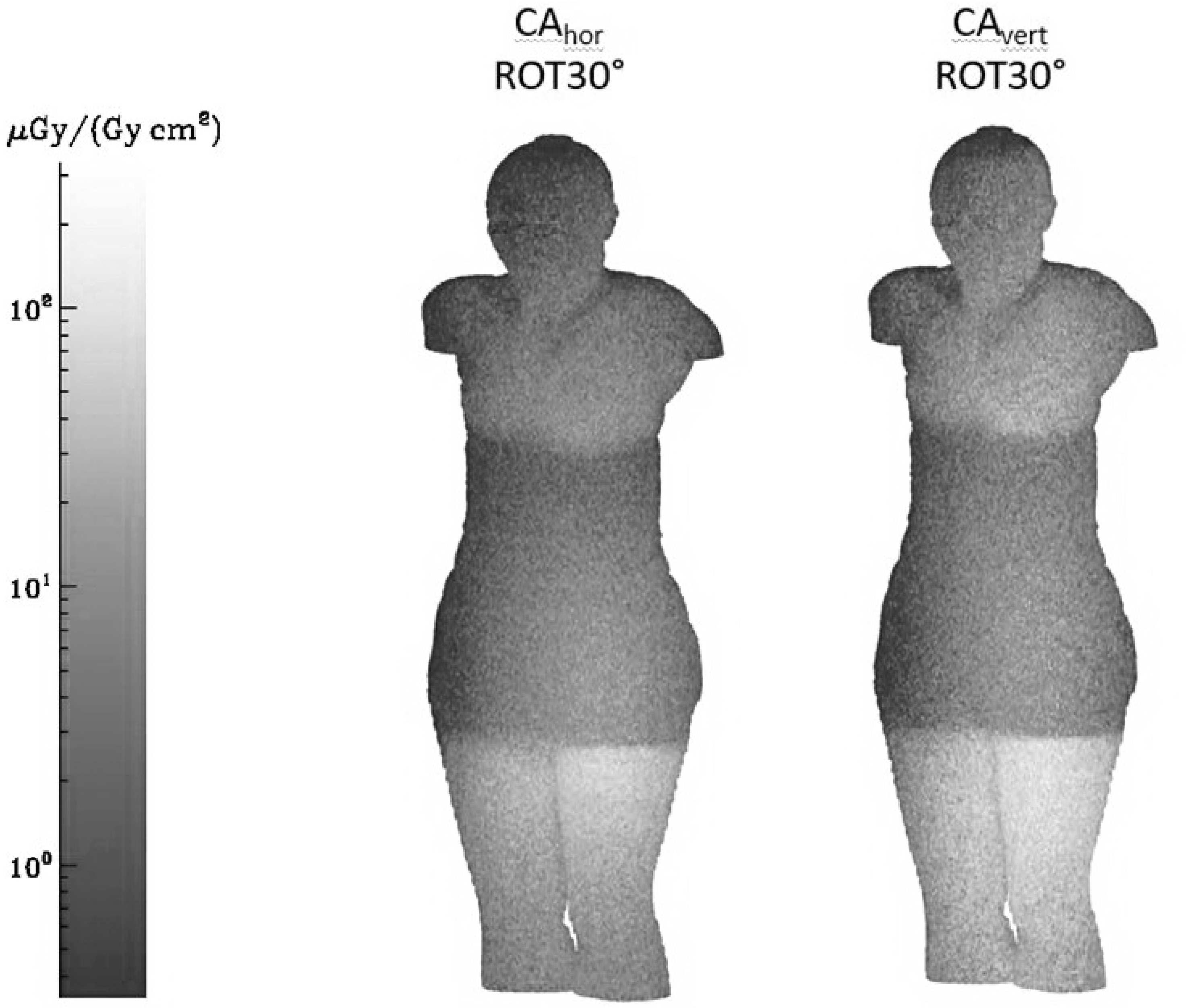

CA$_{hor}$
ROT30°
CA$_{vert}$
ROT30°
μGy/(Gy cm²)
10²
10¹
10⁰

Fig. 1 Components of X-radiation traversing the shielding material. Vertical incidence occurs only in a selective direction.

Fig. 2 CA_{hor} setup for the measurement of *Hp(10)*-based attenuation factors of X-ray shielding aprons. *Hp(10)* doses were measured with 4 dosimeters at 3 distances/orientations of the Alderson phantom (operator phantom). Dimensions in mm.

Fig. 3 Arrangement of the 4 *Hp(10)* dosimeters mounted on the front of the operator phantom torso

Fig. 4 Cross-section of the Monte Carlo simulation scenario at the central height of the water phantom (87.5cm) for the case of a supine patient being X-rayed (CA_{vert} geometry) and the operator being 30cm away directly facing the patient (frontal incidence). The exposure simulation of the operator is divided into three steps indicated by Roman numerals (see text for more details).

Fig. 5 CA_{hor} and CA_{vert} scenarios were investigated with MC-simulation (schematically). Effective dose *E* was calculated with and without the cylindric shield to get the effective attenuation factors based on *E*.

Fig. 6 Dosimeter readings at 80 kV behind 0.25 mm Pb, operator orientation ROT30°

Fig. 7 Comparison of the attenuation factors of a 0.35 mm Pb apron evaluated from a) MC-simulations based on *E*, b) phantom measurements based on *Hp(10)* and c) IEC standard conditions. Beam geometry: CA_{hor}, operator orientation: ROT30°.

Fig. 8 Visualisation of the skin doses for 100 kV tube voltage under different scenarios behind 0.25 mm Pb protection of a female operator standing 30 cm from the patient. Beam geometry and incidence direction are indicated. The scale bar represents the logarithm of the ratio skin dose operator/DAP patient (µGy/(Gy*cm^2)).

Fig. 9 Visualisation of the skin dose distribution of the female operator at 100 kV. Applied shielding: 0.25 mm Pb all over plus 0.25 mm Pb of the lower body. Beam geometry and operator incidence direction are indicated. Scale bar, see Fig.8.